

Laminar mixed convection in a duct with a backward-facing step: the effects of inclination angle and Prandtl number

B. HONG, B. F. ARMALY and T. S. CHEN

Department of Mechanical and Aerospace Engineering and Engineering Mechanics,
University of Missouri-Rolla, Rolla, MO 65401, U.S.A.

(Received 20 July 1992 and in final form 14 December 1992)

Abstract—Mixed convective heat transfer results for two-dimensional laminar flow in an inclined duct with a backward-facing step are presented for both the buoyancy assisting and the buoyancy opposing flow conditions. The wall downstream of the step is maintained at a uniform heat flux, while the straight wall that forms the other side of the duct is maintained at a constant temperature equivalent to the inlet fluid temperature. The wall upstream of the step and the backward-facing step are considered as adiabatic surfaces. The inlet flow is fully developed and is at a uniform temperature. The effects of the inclination angle and Prandtl number on the velocity and temperature distributions are reported.

INTRODUCTION

A SUDDEN change of wall orientation in flow passages will significantly affect the characteristics of the flow near the wall and sometimes causes flow separations and reattachments. A typical case is flow over a stepped wall where a forward-facing step forms a sudden compression of the flow, while a backward-facing step forms a sudden expansion of the flow. The combination of these two geometries yields a rib or an open cavity. Investigations have shown rapid changes in heat transfer and friction coefficient near a step or a rib, which may provide the potential for optimizing some designs of heat transfer devices, such as cooling systems for electronic components and reactors, cooling passages in turbine blades, combustion chambers, and many other heat exchanging surfaces. A backward-facing step which forms a sudden expansion in the flow passage, causes flow separation and develops a recirculation region behind the step. Owing to its relative simplicity, this geometry has been studied by many investigators. The existence of the recirculation region provides high heat transfer performance near the reattachment point of the separated flow for turbulent flow, as presented by Aung and Goldstein [1] and by Aung and Watkins [2], as well as for laminar flow as presented by Aung [3], Sparrow *et al.* [4], and Sparrow and Chuck [5]. Armaly *et al.* [6] experimentally investigated the hydrodynamic behaviors, such as the reattachment length and the velocity profiles, of a laminar duct flow with a backward-facing step. Others utilized different numerical schemes to study the same problem. Sparrow *et al.* [4] reported on the reattachment length and the location of the maximum heat transfer rate for laminar flow in a channel with a step, by using the vorticity-stream function approach, and Aung *et al.* [7] reported the

effects of initial shear-layer thickness on the heat transfer. Vradis and Van Nostrand [8] reported the effects of variable fluid viscosity, and Ötügen [9] carried out an experiment to show the effects of expansion ratio in turbulent flow. Lin *et al.* [10, 11] studied the buoyancy force effects when the wall behind the step was heated and maintained at a constant temperature. All of the above studies treated the case of uniform wall temperature and only Lin *et al.* [10, 11] considered the effect of buoyancy on the flow and heat transfer characteristics. In many practical cooling or heating applications, however, the buoyancy effects cannot be neglected. Also in some cases, the thermal boundary condition at the wall could be better described by specifying the heat flux at the wall rather than the temperature. None of the previous studies dealt with a buoyancy opposing flow or with the effect of the Prandtl number on the flow and heat transfer behavior.

In the present study, buoyancy-affected (assisting and opposing) laminar mixed convection flow over a backward-facing step in a two-dimensional duct with a heated wall subjected to uniform heat flux (UHF) is investigated. The effects of inclination angle and Prandtl number on the flow and heat transfer characteristics are studied for buoyancy assisting and opposing flows.

ANALYSIS

Consider a steady-state two-dimensional incompressible laminar flow in an inclined duct with a sudden expansion behind a backward-facing step as shown in Fig. 1. Fluid enters through the smaller end of the duct and leaves through the larger end. It is assumed that the fluid enters the duct with a uniform

NOMENCLATURE

C_f wall friction coefficient defined by $\tau_w/(\rho u_0^2/2)$
 g gravitational acceleration
 Gr_s Grashof number, $g\beta q_w s^4/(k\nu^2)$
 h channel height at inlet
 H channel height at exit
 k thermal conductivity of the fluid
 L_c length of calculation domain, $x_i + x_e$
 Nu_x local Nusselt number, $q_w s/[k(T_w - T_0)]$
 p pressure
 P dimensionless pressure defined by $(p + \rho g x)/(\rho u_0^2)$
 Pr Prandtl number of the fluid, ν/α
 q_w wall heat flux
 R expansion ratio, H/s
 Re_s Reynolds number defined by $u_0 s/\nu$
 s step height
 T fluid temperature
 T_0 temperature of the inlet fluid or the unheated wall
 T_w temperature of the heated wall
 u streamwise velocity component
 u_i local inlet velocity
 u_0 average inlet velocity
 U dimensionless streamwise velocity component, u/u_0
 v transverse velocity component

V dimensionless transverse velocity component, v/u_0
 x streamwise coordinate as measured from the step
 x_e calculation domain downstream of step
 x_i inlet length upstream of step
 x_n location of peak Nusselt number
 x_0 secondary recirculation length
 x_r reattachment length
 X dimensionless streamwise coordinate, x/s
 X_e, X_i, X_n, X_0, X_r $x_e/s, x_i/s, x_n/s, x_0/s, x_r/s$
 y transverse coordinate
 Y dimensionless transverse coordinate, y/s

Greek symbols

α thermal diffusivity of fluid
 β volumetric coefficient of thermal expansion
 γ inclination angle as measured from the vertical axis
 θ dimensionless temperature, $(T - T_0)/(q_w s/k)$
 ν kinematic viscosity of the fluid
 ξ buoyancy parameter, Gr_s/Re_s^2
 ρ density of the fluid
 τ_w local wall shear stress, $\mu(\partial u/\partial y)_{y=w}$
 ψ stream function.

temperature T_0 and with a fully developed velocity profile. The straight wall of the duct is maintained at a uniform temperature that is equal to the inlet fluid temperature T_0 . The upstream portion of the stepped wall and the backward-facing step are treated as adia-

batic surfaces, while the wall downstream of the step is heated and maintained at a uniform heat flux q_w . The inlet length upstream of the step is x_i and the exit length downstream of the step is x_e . The gravitational acceleration g is acting vertically downward, and the calculation domain has a length of $L_c = x_i + x_e$ and a height of $H = h + s$.

In the analysis, the fluid properties (such as thermal diffusivity α , kinematic viscosity ν , and thermal expansion coefficient β) are treated as constant and evaluated at the inlet temperature T_0 . By employing the Boussinesq approximation and introducing the following dimensionless parameters

$$U = u/u_0, \quad V = v/u_0, \quad X = x/s, \quad Y = y/s \quad (1)$$

$$\theta = (T - T_0)/(q_w s/k), \quad P = (p + \rho g x)/\rho u_0^2 \quad (2)$$

$$Pr = \nu/\alpha, \quad Re_s = u_0 s/\nu \quad (3)$$

$$Gr_s = g\beta q_w s^4/k\nu^2 \quad (4)$$

$$Gr_x = Gr_s \cos \gamma, \quad Gr_y = Gr_s \sin \gamma \quad (5)$$

the non-dimensional form of the governing conservation equations for the physical problem described can be written as

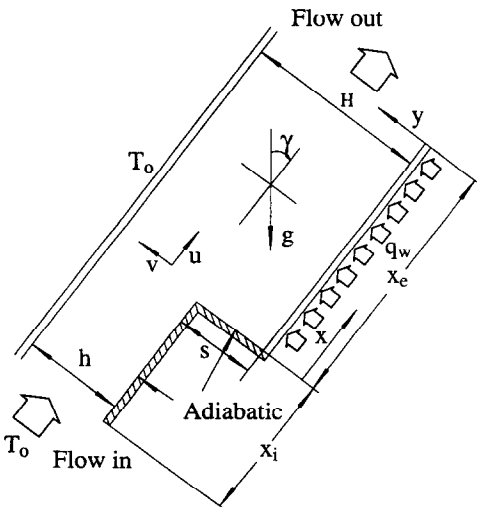


FIG. 1. Schematic diagram of flow domain.

Continuity:

$$U \frac{\partial U}{\partial X} + V \frac{\partial V}{\partial Y} = 0 \quad (6)$$

X-momentum

$$U \frac{\partial U}{\partial X} + V \frac{\partial U}{\partial Y} = - \frac{\partial P}{\partial X} + \frac{1}{Re_s} \left(\frac{\partial^2 U}{\partial X^2} + \frac{\partial^2 U}{\partial Y^2} \right) + \frac{Gr_x}{Re_s^2} \theta \quad (7)$$

Y-momentum

$$U \frac{\partial V}{\partial X} + V \frac{\partial V}{\partial Y} = - \frac{\partial P}{\partial Y} + \frac{1}{Re_s} \left(\frac{\partial^2 V}{\partial X^2} + \frac{\partial^2 V}{\partial Y^2} \right) + \frac{Gr_y}{Re_s^2} \theta \quad (8)$$

Energy

$$U \frac{\partial \theta}{\partial X} + V \frac{\partial \theta}{\partial Y} = \frac{1}{Pr Re_s} \left(\frac{\partial^2 \theta}{\partial X^2} + \frac{\partial^2 \theta}{\partial Y^2} \right) \quad (9)$$

The last term on the right-hand-side of the momentum equations (7) and (8) represents the buoyancy force contribution which could become significant when the Reynolds number is relatively low and the Grashof number is relatively high, as shown by Lin *et al.* [10]. The governing equations for the pure forced convection case for this geometry are the same as the above equations with the exception that the last term in equations (7) and (8) are deleted, i.e. there is no coupling between the momentum and the energy equations.

The boundary conditions for the above set of governing equations are:

(i) Upstream inlet conditions at $X = -X_i$ and $1 \leq Y \leq R$, where $R = H/s$:

$$U_i = u_i/u_0, \quad V = 0, \quad \theta = 0. \quad (10)$$

The flow at the duct inlet is assumed to be fully developed with an average velocity u_0 . Thus, the inlet velocity distribution is parabolic and can be expressed as

$$U_i|_{X=-X_i} = \frac{3}{2} \left[1 - \left(\frac{R+1-2Y}{R-1} \right)^2 \right] \quad (11)$$

(ii) Downstream exit conditions at $X = X_e$ and $0 \leq Y \leq R$:

$$\partial^2 U / \partial X^2 = 0, \quad \partial^2 V / \partial X^2 = 0, \quad \partial^2 \theta / \partial X^2 = 0 \quad (12)$$

(iii) Straight wall at $Y = R$ and $-X_i \leq X \leq X_e$:

$$U = 0, \quad V = 0, \quad \theta = 0 \quad (13)$$

(iv) Stepped wall

Upstream of the step at $Y = 1$ and $-X_i \leq X \leq 0$:

$$U = 0, \quad V = 0, \quad \partial \theta / \partial Y = 0 \quad (14)$$

At the step $X = 0$ and $0 \leq Y \leq 1$:

$$U = 0, \quad V = 0, \quad \partial \theta / \partial X = 0 \quad (15)$$

Downstream of the step at $Y = 0$ and $0 < X \leq X_e$:

$$U = 0, \quad V = 0, \quad \partial \theta / \partial Y = -1. \quad (16)$$

The dimensionless conservation equations and the boundary conditions show that all quantities related to this problem are function of Pr , Re_s , Gr_s , θ , R , X , Y , X_i , and X_e . Since the wall upstream of the step is adiabatic and the flow entering the duct, at $X = -X_i$, is fully developed, the effect of X_i was found to be negligible when $X_i \geq 5$. Similarly, the effect of X_e was also found to be negligible when $X_e \geq 30$. In this study the results will focus on the effect of inclination angle and the Prandtl number on the flow and heat transfer characteristics. All the other parameters will be fixed at $Re_s = 100$, $Gr_s = 609$ and $R = 2$. These magnitudes result from an air flow at 293 K with $s = 0.0048$ m, $H = 0.0096$ m, $u_0 = 0.314$ m s⁻¹, and $q_w = 200$ W m⁻². The effects of Reynolds number, Grashof number and the expansion ratio on the flow and heat transfer characteristics have already been reported by Hong *et al.* [12] for air flow in the vertical geometry. The results of that study show that increasing the Reynolds number increases the reattachment length and the Nusselt number, but it decreases the friction coefficient; increasing the Grashof number will increase the wall friction coefficient and the Nusselt number, but it decreases the reattachment length; increasing the expansion ratio will increase the reattachment length when the expansion ratio is less than 2.25, but decreases it when the expansion ratio is higher than 2.25.

NUMERICAL PROCEDURE

Since the buoyancy force term appears in the momentum equations, the thermal field and the flow field are coupled, and they have to be solved simultaneously. The SIMPLE algorithm as described by Patankar [13] was utilized to obtain the solution of the coupled partial differential equations. The initial velocity and pressure distributions inside the flow domain were set to zero and the initial temperature distribution was set as uniform and equal to the inlet fluid temperature. The momentum equations were solved first based on the temperature and the velocity values from the previous iteration step and then the energy equation was solved to update the temperature field. This process was repeated for each iteration step until a converged solution was obtained. The computer code was verified by predicting the experimental results of Armaly *et al.* [6] and the numerical results of Lin *et al.* [10].

In this study, the entrance length was set to $X_i = 5$ and the length downstream of the step was chosen to be $X_e = 30$. These lengths were selected after establishing the fact that a longer length will essentially not affect the results in the neighborhood of the recir-

ulation region behind the step. A non-uniform grid system was adopted, with grid points of 100 and 50 in the streamwise and transverse directions, respectively. Grid points were distributed such that they were more tightly packed near the walls and near the location of the reattachment point where steep variations of velocities were expected. Trial runs were made to identify more accurately these regions. The grid system was varied smoothly in both the streamwise and the transverse directions, forming the minimum and maximum step sizes of 0.1 and 1.4 in the X direction, and 0.02 and 0.07 in the Y direction, respectively. The number of grid points was also doubled (140×70) in the calculations to assure grid independent solution. The maximum changes in Nu_x , U , and X_r in the recirculation region for these two grid systems are less than 1.2, 5.5, and 0.8%, respectively. The numerical solution was considered as converged when the maximum of the total normalized residuals of mass, momentum and energy was less than 0.01. All computations were performed on an Apollo-10000 computer and it took about 1000 iterations in most cases to reach a converged solution.

RESULTS AND DISCUSSION

To investigate the effects of inclination angle on the flow and heat transfer characteristics, the inclination angle was varied from 0 to 360° while keeping the other parameters constant, i.e. $Re_s = 100$, $Gr_x = 609$, and $R = 2$ and $Pr = 0.712$. Similarly, in investigating the effects of the Prandtl number the inclination angle was fixed at $\gamma = 0$ while varying only the Prandtl number in the range of $0.07 \leq Pr \leq 100$.

Effects of inclination angle

The conservation equations show clearly that changes in the inclination angle influence the magnitude of the buoyancy parameter in both the X and the Y directions. The buoyancy parameter in the X direction, Gr_x/Re_s^2 , and in the Y direction, Gr_y/Re_s^2 , will vary sinusoidally with the inclination angle and the flow will experience buoyancy assisting and buoyancy opposing effects as the inclination angle changes from 0 to 360° . As the inclination angle increases from 0 to 180° the buoyancy force in the X direction decreases, reaching its minimum value at $\gamma = 180^\circ$. As the inclination angle continues to increase from 180 to 360° the buoyancy force in the X direction increases, reaching its maximum value at $\gamma = 0$ or 360° . The general flow characteristics as affected by increasing the inclination angle, γ , from 0 to 360° are illustrated in Fig. 2. The size of the geometries is based on the dimensionless length of the step height. Each of the figures for a given angle γ captures only a small region of the calculation domain to highlight the influence of the inclination angle on the recirculation region and the reattachment length. These individual figures illustrate the changes in the stream function for inclination angles from 0 to 360° . At the vertical position ($\gamma = 0^\circ$),

the streamwise buoyancy component Gr_x has its maximum value, whereas the transverse buoyancy component Gr_y is zero. At this orientation, the buoyancy is assisting the forced flow. The opposite orientation is the downward flow with $\gamma = 180^\circ$, where the transverse buoyancy component Gr_y is again zero but the streamwise buoyancy component Gr_x is opposing the forced flow. The influence of the inclination angle is clearly seen from the changes in the sizes of the primary and the secondary recirculation regions.

A more quantitative illustration of the sizes of the recirculation regions for $0^\circ \leq \gamma \leq 360^\circ$ is shown in Fig. 3. The reattachment length, X_r , increases with increasing inclination angle for $0^\circ \leq \gamma \leq 180^\circ$ and decreases with increasing inclination angle for $180^\circ \leq \gamma \leq 360^\circ$. The length of the secondary recirculation region, X_0 , on the other hand, decreases as the inclination angle increases for $0^\circ \leq \gamma \leq 180^\circ$ and increases as the inclination angle increases for $180^\circ \leq \gamma \leq 360^\circ$. A closer examination of Fig. 3 reveals that the X_r curve as well as the X_0 curve are not entirely symmetric with respect to $\gamma = 180^\circ$, which means that the direction of the transverse buoyancy force influences the sizes of both recirculation regions and that it is responsible for causing the nonsymmetry in these curves. It is clear from these results that placing this geometry at $\gamma = 270^\circ$ would not eliminate the influence of the buoyancy force. This orientation has been selected by some investigators (i.e. Aung [3]) to experimentally measure the forced convection behavior in this geometry with the hope of eliminating the buoyancy force effects. Figure 3 also shows that the influence of the inclination angle decreases as the Prandtl number increases and also as the Grashof number, Gr_x , decreases. In addition, the location of the peak Nusselt number, X_n , is seen to increase with increasing inclination angle from 0 to 180° and to decrease as the inclination angle continues to increase from 180 to 360° . The location of the peak Nusselt number, X_n , is upstream of the reattachment point X_r (i.e. $X_n < X_r$) for the region $110^\circ < \gamma < 250^\circ$ and is downstream of it (i.e. $X_n > X_r$) for the inclination angles outside that region.

Correlation equations for the reattachment length X_r , the secondary recirculation length X_0 , the location of the peak Nusselt number X_n , and the maximum Nusselt number $Nu_{s,max}$ as a function of the inclination angle were developed. They are given by

$$X_r = [5.462 - 1.620 \cos(\gamma)][0.95 + 0.05 \cos(2\gamma)][1.0 + 0.02 \sin(\gamma)] \quad (17)$$

$$X_0 = \text{MAX}\{0.4462 \cos(\gamma)[1.0 - 0.50 \sin(\gamma)], 0.0\} \quad (18)$$

$$X_n = [5.472 - 0.6535 \cos(\gamma)][0.98 + 0.02 \cos(2\gamma)][1.0 + 0.02 \sin(\gamma)] \quad (19)$$

and

$$Nu_{s,max} = [1.01 - 0.01 \cos(2\gamma)][1.752 + 0.151 \cos(\gamma)] \quad (20)$$

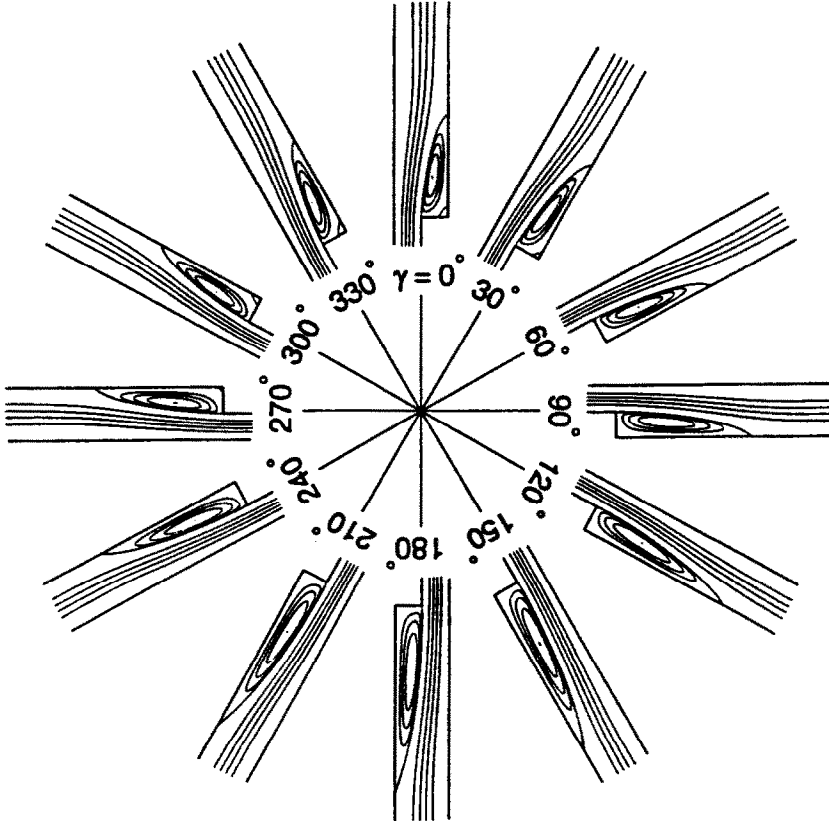


FIG. 2. Streamlines for different inclination angles ($Gr_s = 609$, $Re_s = 100$, $R = 2$ and $Pr = 0.712$).

where $\text{MAX}\{a, b\}$ is a function that returns the larger of the two arguments. The above correlation equations give maximum deviations from the predicted results by 0.04, 0.2, 0.08, and 0.02 respectively.

For the buoyancy assisting cases, $0^\circ \leq \gamma \leq 90^\circ$ and $270^\circ \leq \gamma \leq 360^\circ$, the friction coefficient $Re_s C_f$ at the heated wall increases above the value for the pure

forced convection case, and for the buoyancy opposing cases, $90^\circ \leq \gamma \leq 270^\circ$, the friction coefficient $Re_s C_f$ at the heated wall decreases below the pure forced convection value due to the corresponding increase or decrease in the streamwise buoyancy Gr_x . The influence of the transverse buoyancy Gr_y on $Re_s C_f$ is generally small in the region away from the recirculation region where the streamwise velocity is relatively high, but in the recirculation region, where the streamwise velocity is relatively small, the influence of the transverse buoyancy force is more pronounced.

The effect of inclination angle on the local Nusselt number is illustrated in Fig. 4. The Nusselt number decreases as the inclination angle increases in the range of $0^\circ \leq \gamma \leq 180^\circ$, and it increases with an increase in the inclination angle when $180^\circ \leq \gamma \leq 360^\circ$. The results in this figure show that the dependence of the Nusselt number on the transverse buoyancy is small even in the recirculation region. The largest difference in the magnitude of the Nusselt number for the cases with identical streamwise buoyancy force and identical but opposite transverse buoyancy force, i.e. $\gamma = 45^\circ$ and 315° , occurs in the neighborhood of the maximum Nusselt number region. Although the difference in these two cases is small, the positive transverse buoyancy force, i.e.

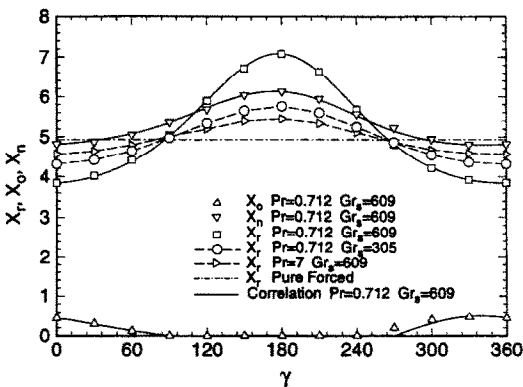


FIG. 3. Inclination angle effects on X_r , X_0 and X_n ($Re_s = 100$ and $R = 2$).

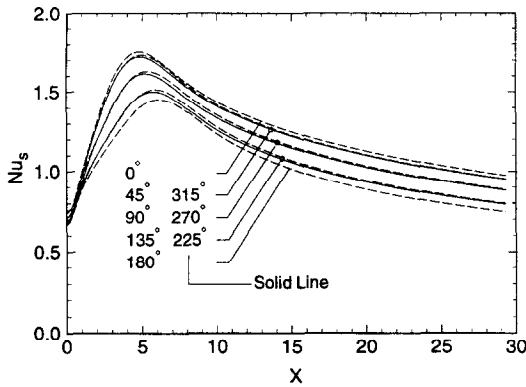


FIG. 4. Inclination angle effects on Nu_s along the heated wall ($Gr_s = 609$, $Re_s = 100$, $R = 2$ and $Pr = 0.712$).

$\gamma = 45^\circ$, results in a higher Nusselt number value than the negative transverse buoyancy force.

The effect of inclination angle on the velocity distributions at $X = 3$ and $X = 25$ is shown in Fig. 5. At $X = 25$, in the vertical orientation the velocity profile is skewed towards the heated wall ($Y = 0$) due to the buoyancy assisting streamwise buoyancy force. By increasing the inclination angle, which is equivalent to changing the magnitude of the streamwise buoyancy force, the peak of the U -velocity profile decreases and its location also moves away from the heated wall and towards the centerline ($Y = 1.0$) of the duct. At $\gamma = 90^\circ$ and 270° , the peak of the velocity profile occurs almost at the centerline of the duct. As the inclination angle continues to increase, $90^\circ \leq \gamma \leq 270^\circ$, in the buoyancy opposing flow regime, the fluid flow in the region adjacent to the heated wall is retarded by the opposing buoyancy force. For these cases, the peak of the velocity profile skews towards the cooler unheated wall ($Y = 2.0$) to maintain mass conservation. Here again the transverse buoyancy force does not play a significant role on the velocity field. However, inside the recirculation region at $X = 3$, where the flow velocity is relatively small in the region near the wall, the transverse buoyancy force plays a more significant role. This figure for $X = 3$ illustrates the increase in the reattachment length and the magnitude of the velocity in the recirculation region as the inclination

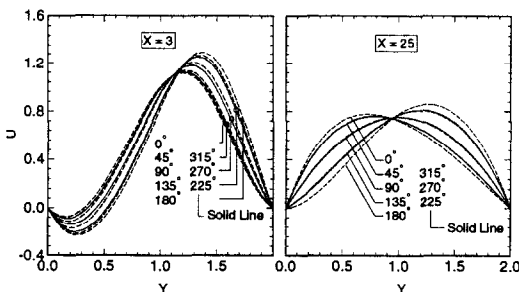


FIG. 5. Inclination angle effects on U at $X = 3$ and 25 ($Gr_s = 609$, $Re_s = 100$, $R = 2$ and $Pr = 0.712$).

angle increases from $\gamma = 0$ to $\gamma = 180^\circ$. The peak velocity increases and the velocity profile skews towards the unheated wall as the inclination angle increases from $\gamma = 0^\circ$ to $\gamma = 180^\circ$.

The temperature distributions exhibit the normal trend of decreasing from the heated wall value to the unheated wall value at any cross-section of the duct. The temperature gradient at the heated wall is constant due to the imposed uniform heat flux condition. The lowest wall temperature occurs for buoyancy-assisting vertical orientation ($\gamma = 0^\circ$), while the highest wall temperature occurs for buoyancy-opposing vertical orientation ($\gamma = 180^\circ$). The transverse buoyancy force has very small effect on the temperature distribution in the region downstream of the reattachment point, but it has some effect on the temperature distribution in the recirculation region where the velocity is low. To conserve space, the temperature profiles are not illustrated.

Effects of Prandtl number

The influence of Prandtl number on the flow and heat transfer characteristics is examined for only one inclination angle corresponding to the case of buoyancy-assisting vertical flow ($\gamma = 0^\circ$). Similar trends will exist for other inclination angles. Figure 6 displays the effect of Prandtl number on the streamlines as well as the isotherms in the region near the step for $Re_s = 100$, $Gr_s = 609$, and $R = 2$. The flow with small Prandtl numbers, i.e. $Pr = 0.07$, is strongly affected by the buoyancy force, thus creating another reverse flow region near the unheated wall to compensate for the accelerated flow in the region near the heated wall. This reverse flow region does not exist when the Prandtl number is large. Also, the size of the primary recirculation region increases, while the size of the secondary recirculation region decreases, with increasing Prandtl number. As in other mixed convection flows, fluids with a smaller Prandtl number are more easily affected by the buoyancy force. The isotherms illustrate the temperature field in the separated flow region. The first line from the cold wall is the line with $\theta_1 = 0.01335$ for all the Prandtl numbers presented in this figure. The most significant information in these plots is the shifting of the θ_1 line for the different Prandtl numbers. For the case of $Pr = 0.07$ this line moves towards the cold wall where $\theta_0 = 0$. With increasing Prandtl number, that line moves towards the heated wall. The area enclosed between the θ_1 line and the heated wall can be considered as the thermally influenced region of the fluid by the heated wall. The large region that is associated with a smaller Prandtl number indicates the relatively strong thermal conduction component in these fluids.

Figure 7 shows the variation of the reattachment length X_r , the length of the secondary recirculation region X_0 , and the location of the peak Nusselt number X_n with the Prandtl number. For small Prandtl number fluids (at this level of buoyancy parameter),

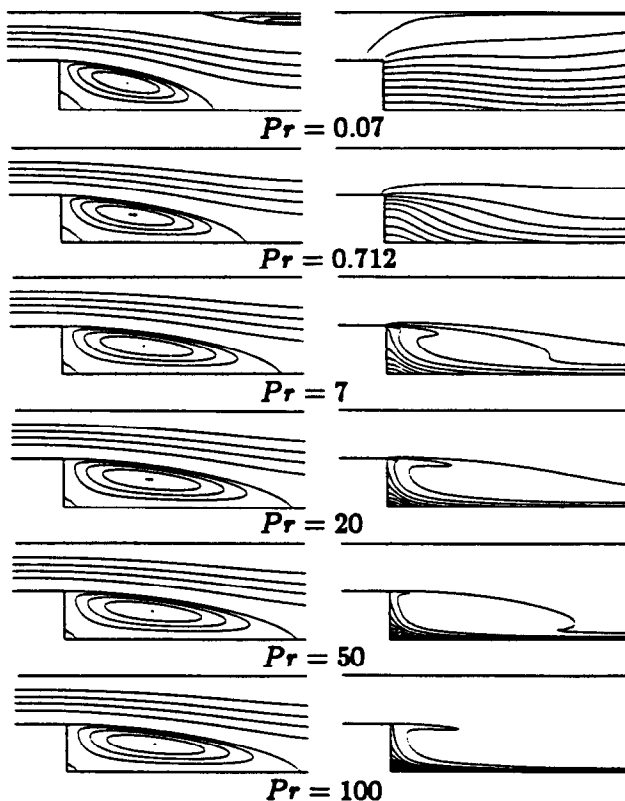


Fig. 6. Streamlines and isotherms for different Prandtl numbers ($\gamma = 0^\circ$, $Gr_s = 609$, $Re_s = 100$ and $R = 2$).

the reattachment length is only about 65% of that for the pure forced convection case. However, for large Prandtl number fluids, say $Pr > 20$, the reattachment length is about 99% of that for the pure forced convection. The size of the secondary recirculation region decreases only slightly with increasing Prandtl number. These behaviors are consistent with the observations that low Prandtl number fluids are affected more by the buoyancy force due to the large thermally affected region as seen in Fig. 6. The

location of peak Nusselt number is downstream of the reattachment point ($X_n > X_r$) for small Prandtl number fluids ($Pr < 10$) and upstream of the reattachment point ($X_n < X_r$) for higher Prandtl number fluids ($Pr > 10$) for the conditions considered in this study.

Correlation equations for the reattachment length X_r , the secondary recirculation length X_0 , the location of the peak Nusselt number X_n , and the maximum Nusselt number $Nu_{s,max}$ as a function of Prandtl number were developed for this part of the study. They are given by

$$X_r = 4.9 - 1.7 \exp(-Pr/0.4) \quad (21)$$

$$X_0 = 0.336 - 0.00165Pr \quad (22)$$

$$X_n = 3.53 + 1.71Pr, \quad 0.07 \leq Pr \leq 0.712 \quad (23a)$$

$$X_n = 4.753 - 0.0091Pr + 6.786 \times 10^{-5}Pr^2, \quad 0.712 < Pr \leq 100 \quad (23b)$$

and

$$Nu_{s,max} = 0.52 + 1.29\sqrt{Pr}. \quad (24)$$

These correlations give maximum deviations of 0.77, 0.15, 0.06, 0.06 and 0.17, respectively, from the predicted results.

In general, the friction coefficient, $Re_s C_f$, increases

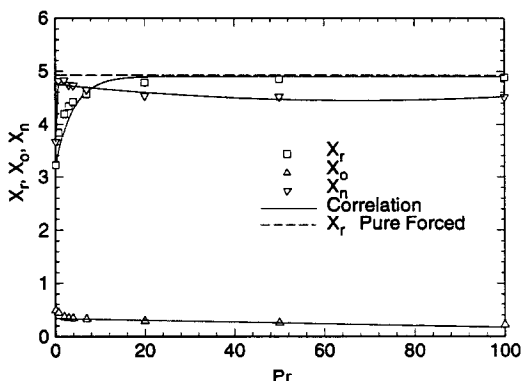


FIG. 7. Prandtl number effects on X_r , X_0 and X_n ($\gamma = 0^\circ$, $Gr_s = 609$, $Re_s = 100$ and $R = 2$).

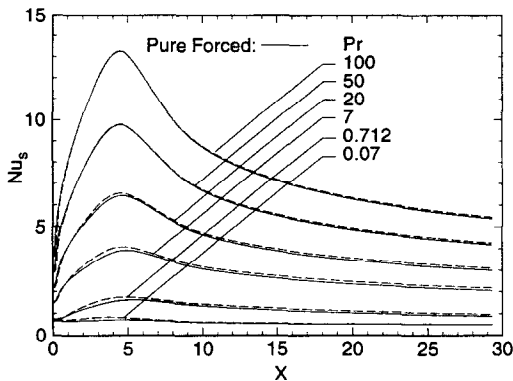


FIG. 8. Prandtl number effects on Nu_s ($\gamma = 0^\circ$, $Gr_s = 609$, $Re_s = 100$ and $R = 2$).

with decreasing Prandtl number because smaller Prandtl number fluids give rise to a higher velocity gradient at the heated wall. The difference between the shear stress for pure forced convection and that for mixed convection decreases with increasing Prandtl number. This supports the previous observations that the buoyancy force effects decrease as the Prandtl number increases. The Nusselt number variation along the heated wall for fluids with different Prandtl numbers is presented in Fig. 8. The Nusselt number increases, whereas the heated wall temperature decreases, as the Prandtl number increases. Also, it can be seen that fluids with a larger Prandtl number give rise to a higher rate of change in the Nusselt number near the step and also a larger magnitude. This behavior is due to the different heat conduction rates in both the streamwise and the transverse directions for fluids with different Prandtl numbers. The nearly flat curves that are associated with low Prandtl numbers reflect the strong streamwise conduction rate that reduces the streamwise temperature gradient in the fluid. The reverse is true for the higher Prandtl number fluids. The buoyancy force does not play an important role on the Nusselt number variation for the Grashof and Reynolds number considered in this part of the study.

The effect of Prandtl number on the velocity distributions at $X = 3$ and 25 is illustrated in Fig. 9. The

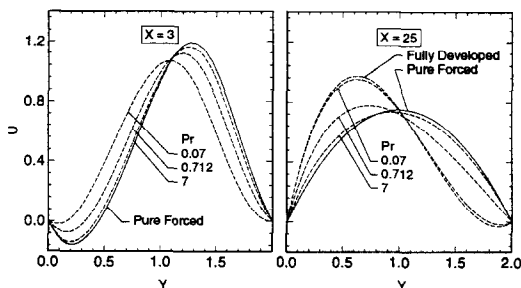


FIG. 9. Prandtl number effects on U at $X = 3$ and 25 ($\gamma = 0^\circ$, $Gr_s = 609$, $Re_s = 100$ and $R = 2$).

distributions for fluids with $Pr > 7$ lie in between those with $Pr = 7$ and that of pure forced convection flow. A high Prandtl number fluid provides a very thin thermally affected region, causing the buoyancy effect to be confined to this thin region adjacent to the heated wall. For this reason the velocity profile for high Prandtl number fluids approaches the pure forced convection flow. For fluids with a smaller Prandtl number, the thermally affected region expands from the heated wall to the cold wall and so does the region that is affected by the buoyancy force. For example, in the case of the flow with $Pr = 0.07$ the velocity profile at the location $X = 25$ approaches the fully developed mixed convection profile. The figure shows that the length of the recirculation region increases as the Prandtl number increases. Also, the wall temperature increases with decreasing Prandtl number, and low Prandtl number fluids reach the fully developed state at smaller streamwise locations than fluids with higher Prandtl numbers.

CONCLUSIONS

The effects of the inclination angle and the Prandtl number on the flow and heat transfer characteristics of two-dimensional laminar mixed convection flow in a duct with a backward-facing step are reported for the case when the downstream wall behind the step is maintained at constant heat flux. Increasing the inclination angle from 0 to 180° will increase the reattachment length, but it will decrease the wall friction coefficient and the Nusselt number at the heated wall. The transverse buoyancy force does not have a significant effect on the flow and heat transfer. Increasing the Prandtl number will increase the Nusselt number and the reattachment length, but it will decrease the wall friction coefficient. Fluids with a smaller Prandtl number are more sensitive to changes in the buoyancy force and will reach the fully developed condition at a smaller downstream location than fluids with a higher Prandtl number.

Acknowledgement—The present study was supported by the National Science Foundation under the grant NSF CTS 8923010.

REFERENCES

1. W. Aung and R. J. Goldstein, Heat transfer in turbulent separated flow downstream of a reattachment step, *Isr. J. Technol.* **10** (1–2), 35–41, (1972).
2. W. Aung and C. B. Watkins, Heat transfer mechanism in separated forced convection. In *Turbulent Forced Convection in Channels and Bundles* (Edited by S. Kakac and D. B. Spalding), Vol. 1, pp. 233–257. McGraw-Hill, New York, (1979).
3. W. Aung, An experimental study of laminar heat transfer downstream of backsteps, *J. Heat Transfer* **105**, 823–829 (1983).
4. E. M. Sparrow, S. S. Kang and W. Chuck, Relation between the points of flow reattachment and maximum heat transfer for regions of flow separation, *Int. J. Heat Mass Transfer* **30**, 1237–1246 (1987).
5. E. M. Sparrow and W. Chuck, PC solutions for heat

- transfer and fluid flow downstream of an abrupt, asymmetric enlargement in a channel, *Numer. Heat Transfer* **12**, 19–40 (1987).
6. B. F. Armaly, F. Durst, J. C. F. Pereira and B. Schounung, Experimental and theoretical investigation of backward facing step flow, *J. Fluid Mech.* **127**, 473–496 (1983).
 7. W. Aung, A. Baron and F. K. Tsou, Wall independency and effect of initial shear-layer thickness in separated flow and heat transfer, *Int. J. Heat Mass Transfer* **28**, 1757–1771 (1985).
 8. G. Vradis and L. Van Nostrand, Laminar flow and heat transfer down-stream of a confined backward facing step including variable viscosity effects, *Simulation and Numerical Methods in Heat Transfer*, ASME, HTD, **157**, 1–8 (1990).
 9. M. V. Ötügen, Expansion ratio effects on the separated shear layer and reattachment downstream of a backward-facing step, *Experiments in Fluids* **10**, 273–280 (1991).
 10. J. T. Lin, B. F. Armaly and T. S. Chen, Mixed convection in buoyancy-assisting, vertical backward-facing step flows, *Int. J. Heat Mass Transfer* **33**, 2121–2132 (1990).
 11. J. T. Lin, B. F. Armaly and T. S. Chen, Mixed convection heat transfer in inclined backward-facing step flows, *Int. J. Heat Mass Transfer* **34**, 1568–1571 (1991).
 12. B. Hong, B. F. Armaly and T. S. Chen, Mixed convection in a duct with a backward-facing step—Uniform heat flux case, *Fundamentals of Mixed Convection*, ASME HTD-Vol. 213, 73–78 (1992).
 13. S. V. Patanker, *Numerical Heat Transfer and Fluid Flow*. Hemisphere, New York, (1980).